JOURNAL OF AEROSPACE INFORMATION SYSTEMS
Vol. 17, No. 9, September 2020

Check for updates

Estimation of Thermal-Conductivity Coefficients in the Global Ionosphere–Thermosphere Model

Ankit Goel,* Brandon Ponder,† Aaron Ridley,‡ and Dennis S. Bernstein§
University of Michigan, Ann Arbor, Michigan 48109

https://doi.org/10.2514/1.I010819

This paper uses retrospective cost parameter estimation (RCPE) to estimate parameters in the global ionosphere–thermosphere model (GITM). Using GITM as an executable simulation code, RCPE estimates two thermal-conductivity coefficients along with the temperature exponent in the thermal-conductivity model. These parameter estimates are obtained by using various combinations of simulated measurements of the global minimum, global maximum, and mean neutral density at a fixed altitude. RCPE is implemented within recursive least squares using both constant-rate forgetting and variable-rate forgetting. The goal of this comparison is to assess the effect of variable-rate forgetting on the convergence of the parameter estimates. The contribution of the paper is thus an investigation of the effectiveness of RCPE for parameter estimation in GITM.

Downloaded by UNIV OF MICHIGAN on July 23, 2022 | http://arc.aiaa.org | DOI: 10.2514/1.I010819

Nomenclature

e_i	=	ith column of the identity matrix
G_f	=	filter
N_i	=	filter coefficient
$\mathcal{O}_p$	=	permutation matrix
$\boldsymbol{q}$	=	forward-shift operator
S	=	temperature exponent
u	=	measured input
y	=	measured output
$\hat{y}$	=	computed output
z	=	output error
κ_i	=	thermal-conductivity coefficient of the ith species, $\mathrm{J \cdot m^{-1} \cdot s^{-1} \cdot K^{-1}}$
λ_c	=	thermal conductivity, $\mathrm{J \cdot m^{-1} \cdot s^{-1} \cdot K^{-1}}$
λ_k	=	forgetting factor
μ	=	unknown parameter
$\hat{\mu}$	=	parameter estimate
ν	=	parameter preestimate
ρ	=	neutral density, $\mathrm{kg \cdot m^{-3}}$

Subscripts

f	=	filter
k	=	iteration step
p	=	permutation

I. Introduction

EMPIRICAL modeling of a physical system entails 1) choosing a suitable model structure, and 2) estimating the parameters within the chosen model structure. Numerous techniques have been developed for parameter estimation. Within the context of state estimation, where parameters can be viewed as constant or slowly varying states, the extended Kalman filter (EKF), unscented Kalman filter (UKF), and ensemble Kalman filter (ENKF) can be used [1–8]. Alternatively, variational methods are applicable [9–11]. Each of these techniques requires either a linearized model (EKF), an adjoint model (variational methods), or an ensemble of models (ENKF, UKF).

An alternative approach to parameter estimation, developed in Ref. [12], relies on a single implementation of an executable simulation code, and thus circumvents the need for either a linearized model, an ensemble of models, or an adjoint model. In particular, retrospective cost parameter estimation (RCPE) uses adaptive integrators to recursively update parameter estimates based on the output error. Since RCPE uses no explicit modeling information, it has no information about how to associate each parameter estimate with the corresponding true parameter. For example, if the system has three unknown parameters, then RCPE produces three parameter estimates; however, only one of the six ($3! = 6$) possible permutations of the parameter estimates correctly associates each parameter estimate with the corresponding true parameter. The correct permutation must therefore be determined based on the output error. With this proviso, RCPE is convenient for parameter estimation in high-dimensional complex physics models that exist only in the form of an executable simulation code whose internal variables are not accessible by the user.

The goal of the present paper is to investigate the effectiveness of RCPE for parameter estimation in a model of the ionosphere–thermosphere. The physics of the ionosphere–thermosphere are complex due to tightly coupled dynamic models [13–15]. These models capture diverse phenomena at various time and length scales based on a combination of first-principles physics and latent variables. For some of these phenomena, a variety of models have been proposed. For example, thermodiffusion models and their coefficients are surveyed in Ref. [16], where more than 20 parameters are used to model the diffusion rate of the neutral atmospheric gases.

The present paper focuses on the global ionosphere–thermosphere model (GITM) developed in Ref. [13]. This model solves coupled continuity, momentum, and energy equations; and it computes neutral, ion, and electron temperatures, neutral-wind and plasma velocities, and mass and number densities of neutrals, ions, and electrons in the upper atmosphere. GITM uses a uniform grid in latitude with a width of $2\pi/n_{\mathrm{lat}}$ rad, where n_{lat} is the number of grid points, and a stretched grid in longitude and altitude to account for temperature and density variations. GITM is implemented in parallel, where the computational domain comprising the atmosphere from 100 to 600 km is divided into blocks. Each block, which is solved on one processor, contains 113,400 states in 4050 cells: each of which contains 28 states. With four blocks solved on a 2×2 grid, GITM entails approximately 500,000 states on a four-processor machine.

The complexity of GITM code precludes the use of linearization, ensembles, and adjoints. Ensemble-based data assimilation for

Received 13 November 2019; revision received 2 April 2020; accepted for publication 9 April 2020; published online 8 May 2020. Copyright © 2020 by Ankit Goel. Published by the American Institute of Aeronautics and Astronautics, Inc., with permission. All requests for copying and permission to reprint should be submitted to CCC at www.copyright.com; employ the ISSN 2327-3097 (print) or 2327-3097 (online) to initiate your request. See also AIAA Rights and Permissions www.aiaa.org/randp.

*Research Fellow, Department of Aerospace Engineering, 1320 Beal Ave.; ankgoel@umich.edu.

†Ph.D. Candidate, Department of Climate and Space Sciences and Engineering, 2455 Hayward St; bponder@umich.edu.

‡Professor, Department of Climate and Space Sciences and Engineering, 2455 Hayward St; ridley@umich.edu.

§Professor, Department of Aerospace Engineering, 1320 Beal Ave.; dsbaero@umich.edu.

Downloaded by UNIV OF MICHIGAN on July 23, 2022 | http://arc.aiaa.org | DOI: 10.2514/1.1010819

GITM was considered in Ref. [17]; however, the programming complexity and computation cost were extremely high. More generally, ensemble-based methods require data exchange among processors at every step in order to update the parameter estimates, which increase the computational cost in terms of time and memory, and require considerable programming effort. In contrast, RCPE uses the output error computed based on the previous parameter estimate in order to update the parameter estimate, and thus obviates the need for data exchange among processors.

Using GITM as an executable simulation code, the present paper estimates two thermal-conductivity coefficients along with the temperature exponent in the thermal-conductivity model. These estimates are obtained by using various combinations of simulated measurements of the global minimum, global maximum, and mean neutral density at a fixed altitude. The range of cases considered demonstrates the effect of the lack of identifiability that may occur due to insufficient measurements.

RCPE is implemented within recursive least squares (RLS) using both constant-rate forgetting and variable-rate forgetting. The goal of this comparison is to assess the effect of variable-rate forgetting on the convergence of the parameter estimates. The contribution of this paper is thus an investigation of the effectiveness of RCPE based on RLS with variable-rate forgetting for parameter estimation in GITM.

The contents of the paper are as follows. In Sec. II, the role of thermal conductivity in GITM is described. Section III describes the RCPE algorithm. Numerical examples demonstrating the application of RCPE to estimate unknown parameters in GITM are presented in Sec. IV. Finally, conclusions and directions for future work are discussed in Secs. V and VI.

II. Global Ionosphere–Thermosphere Model

GITM solves the Navier–Stokes equations for various neutral constituents and simplified magnetohydrodynamics equations for charged constituents in the upper atmosphere. The species interact with each other through collisions that transfer energy, momentum, and mass in space and among species. These processes (such as chemistry, viscosity, mixing, diffusion, and thermal conduction) are approximated with equations and parameterizations.

The change in temperature at a given level of the atmosphere depends on the vertical temperature gradient described by

$$\frac{\delta T}{\delta t} \propto \frac{\delta}{\delta z}\lambda_c \frac{\delta T}{\delta z} \tag{1}$$

where T is absolute temperature, t is time, and z is altitude. The thermal conductivity λ_c is modeled as

$$\lambda_c = \sum_{i\in\{\mathrm{O},\mathrm{O}_2,\mathrm{N}_2\}} \left(\frac{N_i}{N_{\text{total}}}\right)\kappa_i T^S \tag{2}$$

where κ_i is the thermal-conductivity coefficient of the ith species, N_i is the number density of the ith species, and S is the temperature exponent. The thermal conductivity parameterizes the hydrodynamic transport process that describes the movement of heat through the atmosphere. In GITM, heat is transferred by collisions of the particles in the thermosphere (100 to 600 km). The three main constituents in the thermosphere are molecular nitrogen (N_2) and oxygen (O_2) and atomic oxygen (O), with the molecular species dominating below about 200 km altitude. Therefore, each of these constituents are included in Eq. (2). Furthermore, since the molecular species conduct heat in similar ways, the thermal-conductivity coefficient κ_{N_2} is assumed to be equal to the thermal-conductivity coefficient κ_{O_2} in Eq. (2).

It follows from Eq. (2) that increasing either the thermal-conductivity coefficients or the temperature exponent increases the overall thermal conductivity. This increase in thermal conductivity leads to an increase in the amount of energy distributed to the lower layers of the atmosphere, thus reducing the temperature of the upper thermosphere. This phenomenon was observed in Ref. [18], which also showed large variations in the neutral density corresponding to a change of 10^{-4} J · m^{-1} · s^{-1} · K^{-1} in the thermal-conductivity coefficients. In fact, the same variation in the neutral density corresponds to a change of 10^{-1} in the temperature exponent. To avoid model bias, it is thus necessary to correctly parameterize the thermal conductivity.

The default parameters describing the thermal conductivity in GITM are derived from Ref. [19]. A recent study in Ref. [20], however, proposed an approximation of the thermal conductivity that is more accurate than the model given in Ref. [19]. These conflicting recommendations for parameterizing thermal conductivity emphasize the need for data-driven parameter estimation.

III. Retrospective Cost Parameter Estimation

Consider the discrete-time system

$$x_{k+1} = f(x_k, u_k, \mu) \tag{3}$$

$$y_k = h(x_k, u_k, \mu) \tag{4}$$

where $x_k \in \mathbb{R}^{l_x}$ is the state, $u_k \in \mathbb{R}^{l_u}$ is the measured input, $y_k \in \mathbb{R}^{l_y}$ is the measured output, and $\mu = [\mu_1 \cdots \mu_{l_\mu}]^T \in \mathcal{M} \subseteq \mathbb{R}^{l_\mu}$ is the true parameter, which is unknown. The set $\mathcal{M}$ is assumed to be known and satisfies $\mathcal{M} \subseteq [0, \infty)^{l_\mu}$, that is, $\mathcal{M}$ is contained in the nonnegative orthant. If $\mathcal{M}$ does not satisfy this condition, then $\mathcal{M}$ is replaced by $\mathcal{M}' \triangleq \bar{\mu} + \mathcal{M}$ and μ by $\mu - \bar{\mu}$ in Eqs. (3) and (4), where $\bar{\mu} \in \mathbb{R}^{l_\mu}$ shifts $\mathcal{M}$ such that $\mathcal{M}'$ is contained in the nonnegative orthant. With this transformation, which can always be done if $\mathcal{M}$ is bounded, it can be assumed that μ is an element of the nonnegative orthant. The system [Eqs. (3) and (4)] is viewed as the truth model of a physical system.

Based on Eqs. (3) and (4), the estimation model is constructed as

$$\hat{x}_{k+1} = f(\hat{x}_k, u_k, \hat{\mu}_k) \tag{5}$$

$$\hat{y}_k = h(\hat{x}_k, u_k, \hat{\mu}_k) \tag{6}$$

where $\hat{x}_k$ is the computed state, $\hat{y}_k$ is the computed output of Eqs. (5) and (6), and $\hat{\mu}_k$ is the parameter estimate. It is assumed that f and h are known, and thus they can be used to construct Eqs. (5) and (6). Since the state x is not measured, the initial state x_0 is unknown. Since μ is unknown, it is replaced in Eqs. (5) and (6) by its estimate $\hat{\mu}_k$, which depends on the output error $z_k \in \mathbb{R}^{l_y}$ defined by

$$z_k \triangleq \hat{y}_k - y_k \tag{7}$$

The ability to estimate μ is based on the assumption that Eqs. (3) and (4) are structurally identifiable [21–23] and the data are sufficiently persistent [24,25].

The parameter estimator consists of an adaptive integrator and an output nonlinearity. In particular, the parameter preestimate ν is given by

$$\nu_k = R_k \phi_k \tag{8}$$

where the integrator state $\phi_k \in \mathbb{R}^{l_y}$ is updated by

$$\phi_k = \phi_{k-1} + z_{k-1} \tag{9}$$

The adaptive integrator gain $R_k \in \mathbb{R}^{l_\mu \times l_y}$ is updated by RCPE as will be described in the following. Since ν_k is not necessarily an element of the nonnegative orthant, an output nonlinearity is used to transform ν_k. In particular, the parameter estimate $\hat{\mu}_k$ is given by

$$\hat{\mu}_k = \hat{\mu}_0 + \mathcal{O}_p|\nu_k| \tag{10}$$

where $\hat{\mu}_0$ is the initial guess of μ, $\mathcal{O}_p$ is a permutation matrix that contains exactly one "1" in each of its rows and columns (and the remaining entries are all zero), and the absolute value is applied

componentwise. The parameter estimator, which consists of Eqs. (8–10), is represented in Fig. 1.

To facilitate the subsequent development, note that the parameter preestimate [Eq. (8)] can be rewritten as

$$\nu_k = \Phi_k \theta_k \tag{11}$$

where the regressor matrix Φ_k is defined by

$$\Phi_k \triangleq I_{l_\mu} \otimes \phi_k^T \in \mathbb{R}^{l_\mu \times l_\theta} \tag{12}$$

and the parameter estimator coefficient vector θ_k is defined by

$$\theta_k \triangleq \mathrm{vec} R_k \in \mathbb{R}^{l_\theta} \tag{13}$$

where $l_\theta \triangleq l_\mu l_y$, "$\otimes$" is the Kronecker product, and "vec" is the column-stacking operator. Note that θ_k is an alternative representation of the adaptive integrator gain R_k. Finally, θ_k is chosen as the minimizer of the retrospective cost presented in detail in Ref. [12], and it is given by

$$\lambda_k = \frac{1}{1 + \eta \|z_k\|^\alpha} \tag{14}$$

$$P_{k+1} = \lambda_k^{-1}[P_k - P_k \bar{\Phi}_k^T N^T (\lambda_k I_{l_y} + N \bar{\Phi}_k P_k \bar{\Phi}_k^T N^T)^{-1} N \bar{\Phi}_k P_k] \tag{15}$$

$$\theta_{k+1} = \theta_k - P_{k+1} \bar{\Phi}_k^T N^T [N \bar{\Phi}_k \theta_k + z_k - N \bar{V}_k] \tag{16}$$

where $\eta, \alpha \geq 0$, $P_0 = p_0 I_{l_\theta}$, $\theta_0 = 0$, and

$$N \triangleq [N_1 \ \cdots \ N_{n_f}] \in \mathbb{R}^{l_y \times N_{n_f} l_\mu} \tag{17}$$

$$\bar{\Phi}_k \triangleq \begin{bmatrix} \Phi_{k-1} \\ \vdots \\ \Phi_{k-N_{n_f}} \end{bmatrix} \in \mathbb{R}^{l_\mu N_{n_1} \times l_\theta}, \qquad \bar{V}_k \triangleq \begin{bmatrix} v_{k-1} \\ \vdots \\ v_{k-N_{n_f}} \end{bmatrix} \in \mathbb{R}^{l_\mu N_{n_f}} \tag{18}$$

It is shown in Ref. [12] that the parameter preestimate $\hat{\nu}_k$ is constrained to a subspace defined by the coefficients $N_1, \ldots, N_{n_f}$. In particular,

$$\hat{\nu}_k \in \mathcal{R}([N_1^T \ \cdots \ N_{n_f}^T]) \tag{19}$$

where $\mathcal{R}$ denotes range. Thus, the coefficients $N_1, \ldots, N_{n_f}$ must be chosen such that

$$\mathcal{O}_p(\mu - \bar{\mu}) \in \mathcal{R}([N_1^T \ \cdots \ N_{n_f}^T]) \tag{20}$$

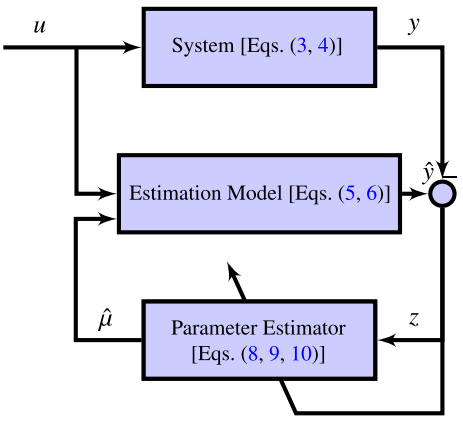

Fig. 1 Retrospective cost parameter estimation.

The integer N_{n_f} is set to be the smallest integer greater than l_μ / l_z, and each row of N_i is chosen to be a row of I_{l_μ} in order to satisfy Eq. (20). As shown numerically in Ref. [12], $\hat{\mu}_k$ converges to μ for at least one choice of the permutation matrix $\mathcal{O}_p$ of the $l_\mu!$ choices.

IV. Thermal-Conductivity Estimation Using Density Measurements

In this section, RCPE is used to estimate the thermal-conductivity coefficients κ_{O_2} and κ_O along with the temperature exponent S in Eq. (2). These estimates are based on simulated measurements of the global minimum, global maximum, and mean neutral density at a fixed altitude.

To obtain neutral-density data, the thermosphere is simulated using GITM from 21 November 2002 to 5 December 2002 with the constant thermal-conductivity coefficients $\kappa_{O_2} = 3.6 \times 10^{-4}$ m^2/s and $\kappa_O = 5.6 \times 10^{-4}$ m^2/s, as well as the temperature exponent $S = 6.9 \times 10^{-1}$. The time step in GITM is 1 s. The neutral density is sampled at intervals of 1 min; thus, the simulated time, which is measured in days, is given by $k/1440$, where $k \geq 0$ is the number of simulated minutes. At each sample time, the global minimum density $\rho_{\min}$, the global maximum density $\rho_{\max}$, and the mean density ρ_{mean} at the altitude of 300 km are computed. These data, which are shown in Fig. 2, are used by RCPE in the following examples. Only the data after 2 h (0.083 days) is used in order to avoid the initial transient. These examples are summarized in Table 1, which specifies the objective of each example. Note that, in all examples presented in this work, noise in the measurements is not considered to focus on the effectiveness of variable-rate forgetting.

To focus on the effectiveness of variable-rate forgetting, noise in the measurements is not considered. However, the effect of noise in RCPE was investigated in Ref. [12].

A. Example IV.1: Estimation of κ_{O_2} Using Measurements of $\rho_{\max}$ with Constant-Rate Forgetting

In this example, measurements of $\rho_{\max}$ are used to construct an estimate $\hat{\mu}_k = \hat{\kappa}_{O_2,k}$ of κ_{O_2}. Therefore,

$$\hat{\kappa}_{O_2,k} = \hat{\kappa}_{O_2,0} + |\nu_k| \tag{21}$$

where $\hat{\kappa}_{O_2,0}$ is the initial estimate of κ_{O_2}, and ν_k is given by Eq. (11). The output of the estimation model is $\hat{y}_k = 10^{10} \hat{\rho}_{\max,k}$, where the scaling ensures that the error z_k and the parameter estimate $\hat{\mu}_k$ have similar magnitude. Let $N_1 = 1$, $p_0 = 10^8$, and the constant-rate forgetting factor $\lambda_k \equiv 0.999$. Figure 3 shows the output error, the estimate $\hat{\kappa}_{O_2,k}$ of κ_{O_2}, and θ_k.

Next, the effect of p_0 on the estimates is investigated. Let $N_1 = 1$ and $\lambda_k \equiv 0.999$. Figure 4 shows the estimate $\hat{\mu}_k = \hat{\kappa}_{O_2,k}$ of κ_{O_2} as well

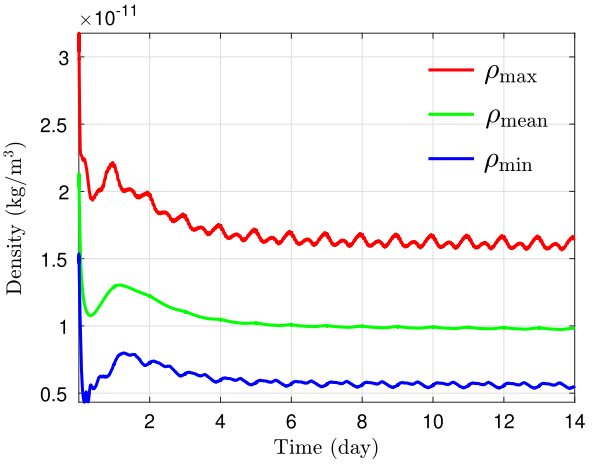

Fig. 2 Simulated neutral-density measurements synthesized using computed neutral density at altitude of 300 km.

Downloaded by UNIV OF MICHIGAN on July 23, 2022 | http://arc.aiaa.org | DOI: 10.2514/1.1010819

Table 1 Summary of the examples in the paper

Example	Estimated Parameters	Measurements	Objectives	Figure
IV.1	κ_{O_2}	ρ_{max}	Constant-rate forgetting, effect of p_0	Figs. 3 and 4
IV.2	κ_O	ρ_{mean}	Variable-rate forgetting, effect of α, η	Figs. 5 and 6
IV.3	κ_{O_2}, κ_O	ρ_{max}	Lack of identifiability due to fewer measurements	Fig. 7
IV.4	κ_{O_2}, κ_O	ρ_{min}, ρ_{max}	Variable-rate forgetting, effect of initialization, effect of filter coefficients	Figs. 8–11
IV.5	κ_{O_2}, κ_O, S	ρ_{min}, ρ_{max}, ρ_{mean}	Variable-rate forgetting, effect of permutation	Figs. 12 and 13

as θ_k for two values of p_0. Note that the larger value of p_0 reduces overshoot but increases the settling time.

B. Example IV.2: Estimation of κ_O Using the Measurements of ρ_{mean} with Variable-Rate Forgetting

In this example, the measurements of ρ_{mean} are used to construct an estimate $\hat{\mu}_k = \hat{\kappa}_{O,k}$ of κ_O. Therefore,

$$\hat{\kappa}_{O,k} = \hat{\kappa}_{O,0} + |\nu_k| \tag{22}$$

where $\hat{\kappa}_{O,0}$ is the initial estimate of κ_O, and ν_k is given by Eq. (11). The output of the estimation model is $\hat{y}_k = 10^{10}\hat{\rho}_{mean,k}$, where the scaling ensures that the error z_k and the parameter estimate $\hat{\mu}_k$ have similar magnitude. Let $N_1 = 1$, $p_0 = 10^8$, and the variable forgetting factor parameters $\alpha = 0.8$ and $\eta = 1.5$. Figure 5 shows the output error, the estimate $\hat{\mu}_k = \hat{\kappa}_{O,k}$ of κ_O, and θ_k.

Next, the effect of α and η on the estimates is investigated. Let $N_1 = 1$ and $p_0 = 10^8$. Figure 6 shows the estimate $\hat{\mu}_k = \hat{\kappa}_{O,k}$ of κ_O as well as θ_k for various values of α and η. Note that larger values of η and smaller values of α reduce overshoot but may increase the settling time.

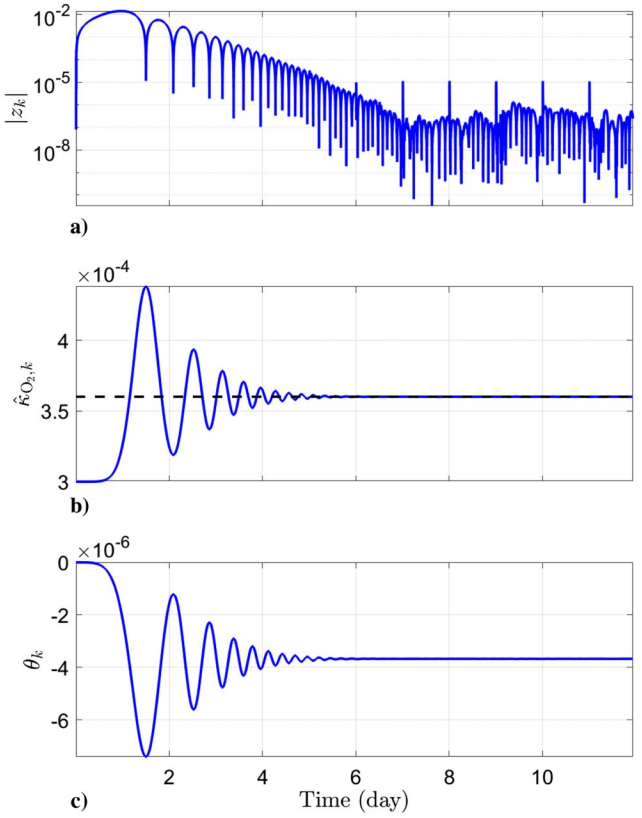

Fig. 3 Example IV.1. Estimation of κ_{O_2} using ρ_{max}: a) output error, b) true parameter and parameter estimate, and c) parameter estimator coefficients.

C. Example IV.3: Estimation of κ_{O_2} and κ_O Using the Measurement of ρ_{max}

In this example, RCPE uses measurement of ρ_{max} to construct the estimates $\hat{\mu}_{1,k} = \hat{\kappa}_{O_2,k}$ and $\hat{\mu}_{2,k} = \hat{\kappa}_{O,k}$ of κ_{O_2} and κ_O. Therefore,

$$\begin{bmatrix} \hat{\kappa}_{O_2,k} \\ \hat{\kappa}_{O,k} \end{bmatrix} = \begin{bmatrix} \hat{\kappa}_{O_2,0} \\ \hat{k}_{0,0} \end{bmatrix} + \mathcal{O}_p|\nu_k| \tag{23}$$

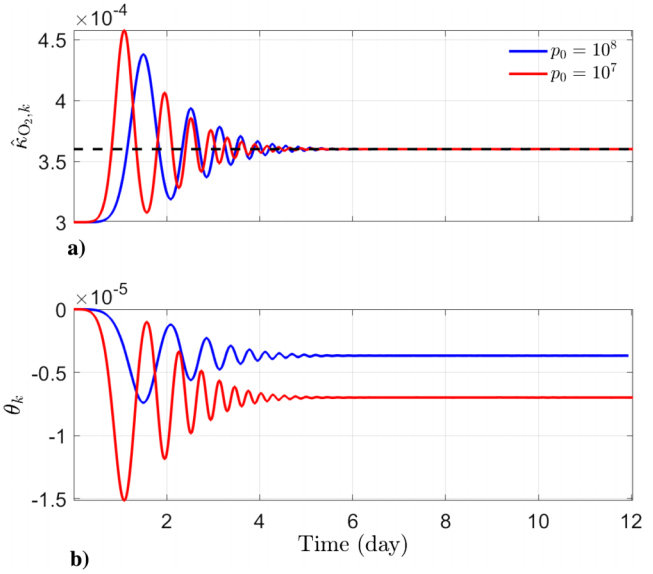

Fig. 4 Example IV.1. Effect of p_0 on the parameter estimates: a) true parameter and parameter estimate, and b) parameter estimator coefficients for two values of p_0.

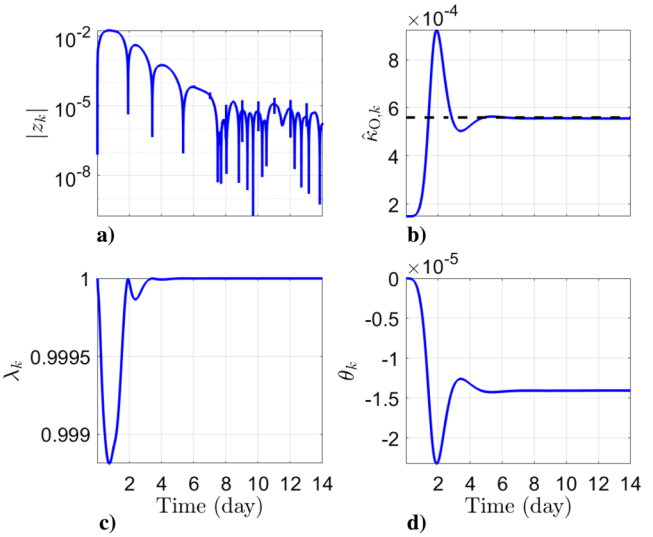

Fig. 5 Example IV.2. Estimation of κ_O using ρ_{mean}: a) output error, b) true parameter and parameter estimate, c) variable-rate forgetting factor, and d) parameter estimator coefficients.

Downloaded by UNIV OF MICHIGAN on July 23, 2022 | http://arc.aiaa.org | DOI: 10.2514/1.1010819

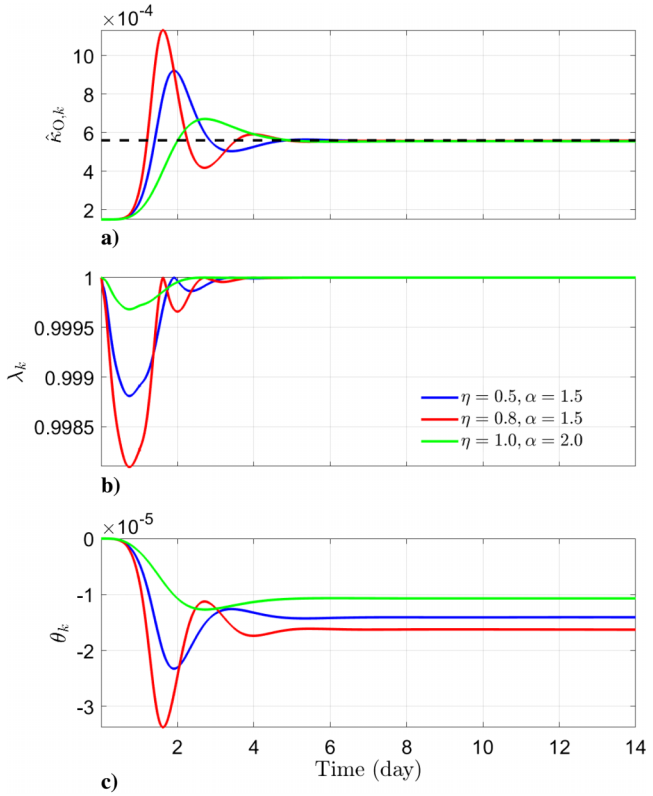

Fig. 6 Example IV.2. Effect of α and η on parameter estimates: a) true parameter and parameter estimate, b) variable-rate forgetting factor, and c) parameter estimator coefficients for several choices of α and η.

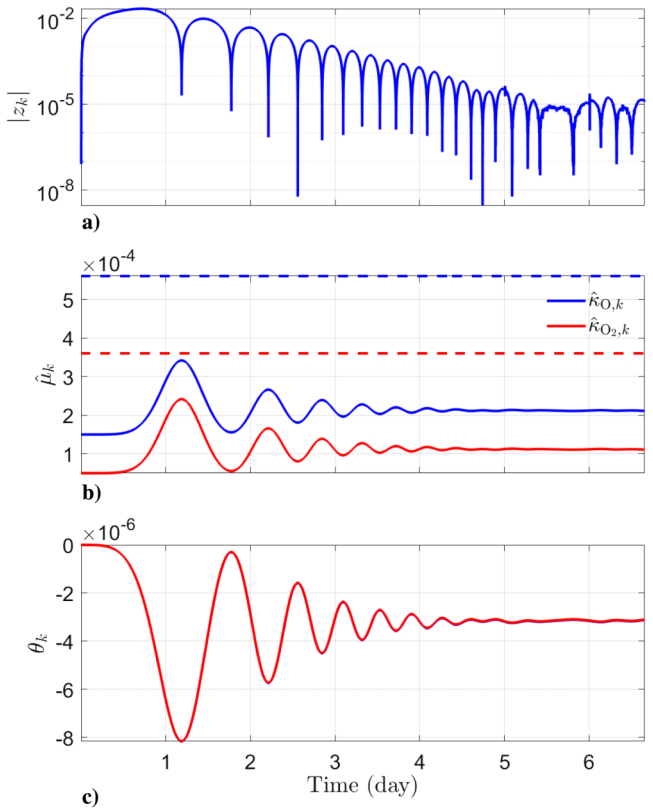

Fig. 7 Example IV.3. Estimation of κ_{O_2} and κ_O using measurements of ρ_{max}: a) output error, b) true parameter and parameter estimate, c) variable-rate forgetting factor, and d) parameter estimator coefficients.

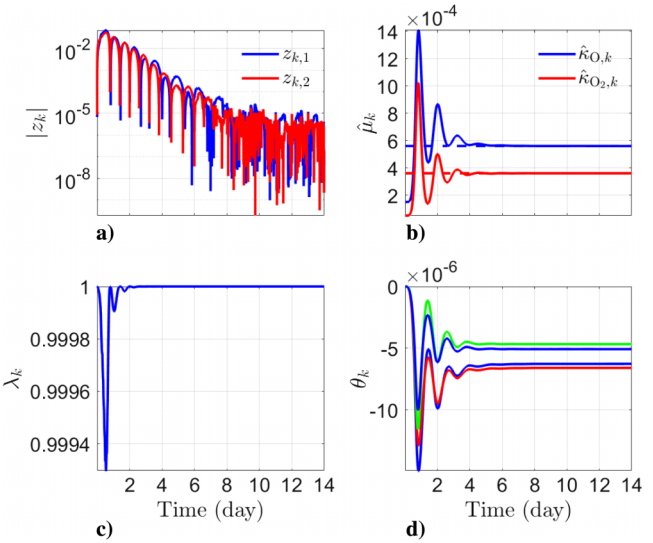

Fig. 8 Example IV.4. Estimation of κ_{O_2} and κ_O using measurements of ρ_{min} and ρ_{max}: a) output error, b) true parameter and parameter estimate, c) variable-rate forgetting factor, and d) parameter estimator coefficients.

where $\hat{\kappa}_{O_2,0}$ is the initial estimate of κ_{O_2}, $\hat{\kappa}_{O,0}$ is the initial estimate of κ_O, $\mathcal{O}_p = I_2$, and ν_k is given by Eq. (11). The output of the estimation model is $\hat{y}_k = 10^{10}\hat{\rho}_{max,k}$, where the scaling ensures that the error z_k and the parameter estimate $\hat{\mu}_k$ have similar magnitude. As shown in Sec. III, estimation of two parameters with a single measurement requires $n_f = 2$ and linearly independent N_1 and N_2. Consequently, RCPE is implemented with $N_1 = e_1^T$, $N_2 = e_2^T$, $p_0 = 10^8$, and $\lambda_k \equiv 0.999$. Figure 7 shows the output error, the estimates $\hat{\mu}_{1,k} = \hat{\kappa}_{O_2,k}$ and $\hat{\mu}_{2,k} = \hat{\kappa}_{O,k}$ of κ_{O_2} and κ_O, and θ_k. Note that the magnitude of the output error z_k reduces by three orders of magnitude; however, the estimate $\hat{\mu}_k$ does not converge to the true values of κ_{O_2} and κ_O, thus suggesting that one measurement is not sufficient to uniquely estimate κ_{O_2} and κ_O.

D. Example IV.4: Estimation of κ_{O_2} and κ_O Using the Measurements of ρ_{min} and ρ_{max}

In this example, measurements of ρ_{min} and ρ_{max} are used to construct the estimate $\hat{\mu}_{1,k} = \hat{\kappa}_{O_2,k}$ and $\hat{\mu}_{2,k} = \hat{\kappa}_{O,k}$ of κ_{O_2} and κ_O.

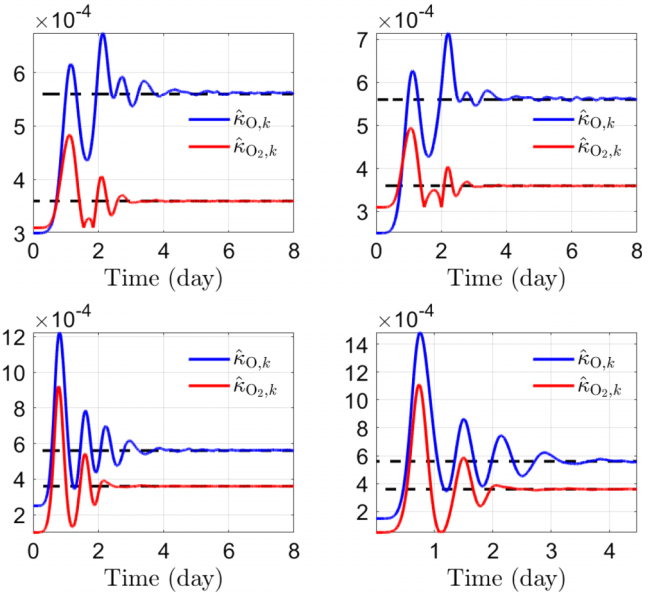

Fig. 9 Example IV.4. Effect of initial estimate of unknown parameter on parameter estimates.

Downloaded by UNIV OF MICHIGAN on July 23, 2022 | http://arc.aiaa.org | DOI: 10.2514/1.1010819

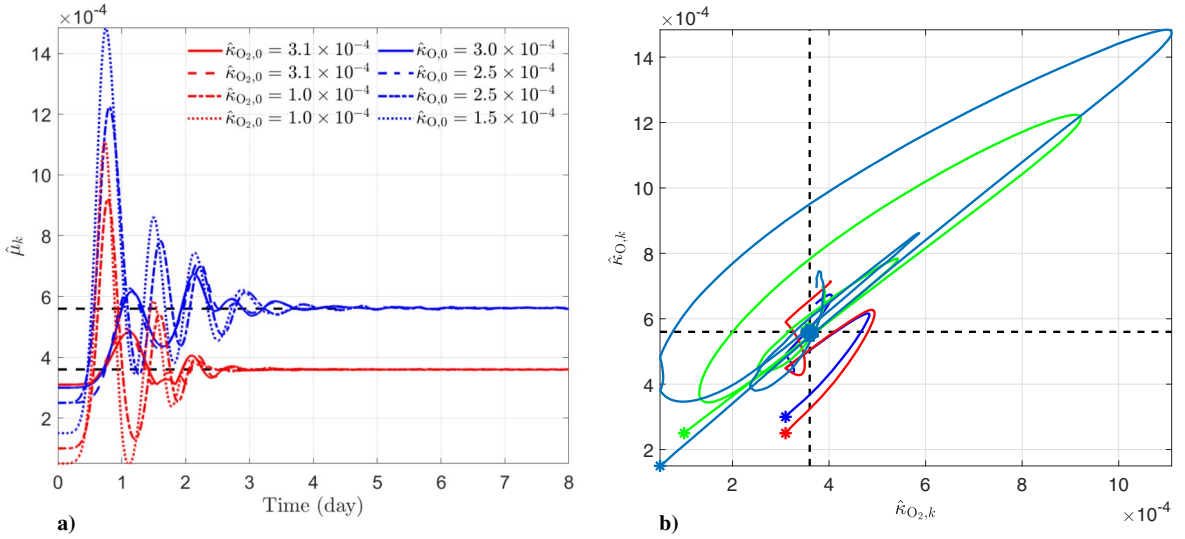

Fig. 10 Example IV.4. Effect of initial estimate of unknown parameter on parameter estimates.

Therefore,

$$\begin{bmatrix} \hat{\kappa}_{O_2,k} \\ \hat{\kappa}_{O,k} \end{bmatrix} = \begin{bmatrix} \hat{\kappa}_{O_2,0} \\ \hat{\kappa}_{O,0} \end{bmatrix} + \mathcal{O}_p |\nu_k| \tag{24}$$

where $\hat{\kappa}_{O_2,0}$ is the initial estimate of κ_{O_2}, $\hat{\kappa}_{O,0}$ is the initial estimate of κ_O, $\mathcal{O}_p = I_2$, and ν_k is given by Eq. (11). The output of the estimation model is $\hat{y}_k = 10^{10}[\hat{\rho}_{\min,k} \quad \hat{\rho}_{\max,k}]^T$, where the scaling ensures that the error z_k and the parameter estimate $\hat{\mu}_k$ have similar magnitude. Let $N_1 = [e_1 \quad e_2]$, $p_0 = 10^8$, and the variable forgetting factor parameters $\alpha = 0.8$ and $\eta = 1.5$. Figure 8 shows the output error, the estimates $\hat{\mu}_{1,k} = \hat{\kappa}_{O_2,k}$ and $\hat{\mu}_{2,k} = \hat{\kappa}_{O,k}$ of κ_{O_2} and κ_O, and θ_k.

Next, the effect of the initial estimate of the unknown parameter on the estimates is investigated. Let $N_1 = [e_1 \quad e_2]$, $p_0 = 10^8$, $\alpha = 0.8$, and $\eta = 1.5$. Figure 9 shows the estimates of κ_{O_2} and κ_O for various values of the initial estimates $\hat{\kappa}_{O_2,0}$ and $\hat{\kappa}_{O,0}$. Figure 10 shows that the overshoot increases as the initial estimate is further away from the true value of the unknown parameters.

Next, the effect of choice of N_1 on the estimates is investigated. With $N_1 = [e_2 \quad e_1]$, Fig. 11 shows the output error, the estimates of κ_{O_2} and κ_O, λ_k, and θ_k. Note that, in this case, both choices of the filter coefficient N_1 were found to be successful.

E. Example IV.5: Estimation of κ_{O_2}, κ_O, and S Using Measurements of $\rho_{\min}$, ρ_{mean}, and $\rho_{\max}$

In this example, measurements of $\rho_{\min}$, ρ_{mean}, and $\rho_{\max}$ are used to construct the estimates $\hat{\mu}_{1,k} = \hat{\kappa}_{O_2,k}$, $\hat{\mu}_{2,k} = \hat{\kappa}_{O,k}$, and $\hat{\mu}_{3,k} = \hat{S}_k$, of κ_{O_2}, κ_O, and the temperature exponent S. Therefore,

$$\begin{bmatrix} \hat{\kappa}_{O_2,k} \\ \hat{\kappa}_{O,k} \\ \hat{S}_k \end{bmatrix} = \begin{bmatrix} \hat{\kappa}_{O_2,0} \\ \hat{\kappa}_{O,0} \\ \hat{S}_0 \end{bmatrix} + \mathcal{O}_p |M\nu_k| \tag{25}$$

where $\hat{\kappa}_{O_2,0}$ is the initial estimate of κ_{O_2}, $\hat{\kappa}_{O,0}$ is the initial estimate of κ_O, $\hat{S}_0$ is the initial estimate of S, $\mathcal{O}_p = I_3$, $M = \text{diag}(1,1,1000)$, and ν_k is given by Eq. (11). Note that the scaling matrix M ensures that all elements of ν_k have similar magnitude. The output of the estimation model is $\hat{y}_k = 10^{10}[\hat{\rho}_{\min,k} \quad \hat{\rho}_{\text{mean},k} \quad \hat{\rho}_{\max,k}]^T$, where the scaling ensures that the error z_k and the parameter estimate $\hat{\mu}_k$ have similar magnitude. Let $N_1 = [e_1 \quad e_2 \quad e_3]$, $p_0 = 10^8$, and the variable

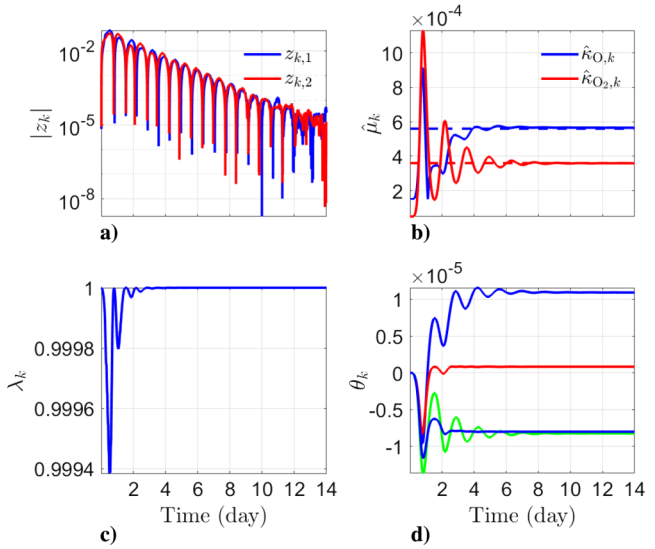

Fig. 11 Example IV.4. Effect of N_1 on the parameter estimates: a) output error, b) true parameter and parameter estimate, c) variable-rate forgetting factor, and d) parameter estimator coefficients using filter coefficient $N_1 = [e_2 \quad e_1]$.

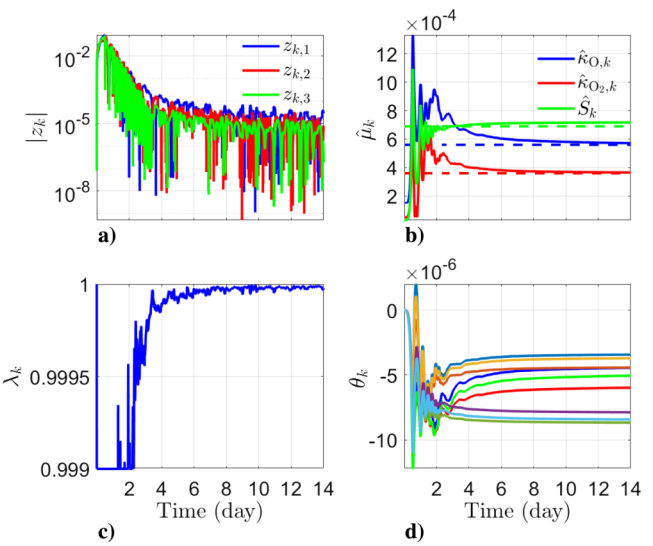

Fig. 12 Example IV.5. Estimation of κ_{O_2} and κ_O using measurements of $\rho_{\min}$ and $\rho_{\max}$: a) output error, b) true parameter and parameter estimate, c) variable-rate forgetting factor, and d) parameter estimator coefficients.

Downloaded by UNIV OF MICHIGAN on July 23, 2022 | http://arc.aiaa.org | DOI: 10.2514/1.1010819

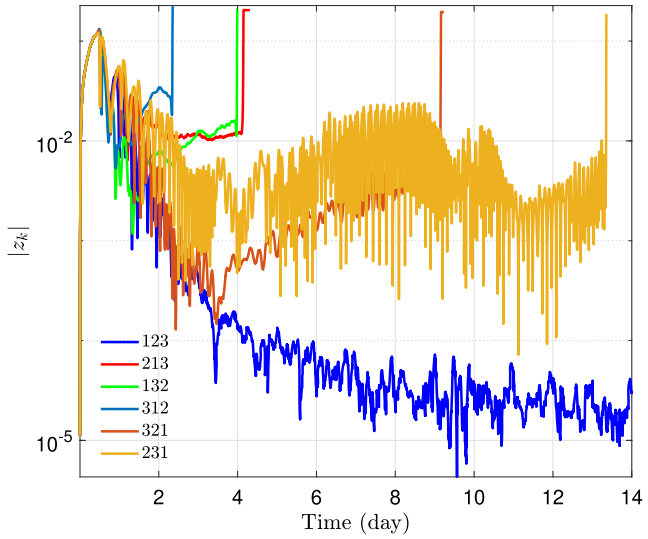

Fig. 13 Example IV.5. Output error for all six permutations of the estimates of κ_{O_2}, κ_O, and S using ρ_{min}, ρ_{max}, and ρ_{mean}. Output error diverges for five of the six permutations.

forgetting factor parameters $\alpha = 0.8$ and $\eta = 1.5$. Figure 12 shows the output error; the estimates of κ_{O_2}, κ_O, and S; λ_k; and θ_k Note that the variable forgetting factor λ_k is lower bounded at 0.999 in this example to prevent excessive forgetting.

Next, the effect of the choice of the permutation matrix $\mathcal{O}_p$ is investigated. For $l_\mu = 3$, there are $3! = 6$ possible choices of $\mathcal{O}_p$. Figure 13 shows the output error for all six choices of p. Note that the output error diverges for all but one choice of p.

V. Future Research

Future research will address four extensions. First, the effect of sensor noise on the accuracy of the parameter estimates within the context of RLS with variable-rate forgetting remains to be investigated. In earlier work, this effect was considered within the context of constant-rate forgetting. Second, the measurements used in the present study were simulated measurements of the maximum, minimum, and mean neutral densities at a fixed altitude. More realistic measurements would be neutral-density data along satellite tracks. Third, in order to facilitate the use of RCPE for estimating a larger number of unknown parameters, it is desirable to reduce the computational cost of RCPE by developing a technique for efficiently determining the correct permutation matrix. Finally, automated techniques for selecting the initial covariance and variable-forgetting-factor parameters α and η would make RCPE more convenient for larger classes of applications.

VI. Conclusions

Based on simulated density measurements, retrospective cost parameter estimation was used to estimate the thermal-conductivity coefficients and the temperature exponent modeling thermal conductivity in the global ionosphere–thermosphere model. A comparison of constant-rate and variable-rate forgettings using a single measurement showed that variable-rate forgetting improves the convergence of the estimator. For the case of two unknown parameters, the output error converged to zero; however, the parameter estimates converged to values that differ from the truth values. For this choice of measurement signal, it thus follows that the underlying physics preclude identifiability of the unknown parameters. Next, for the case where two density measurements were used to estimate two unknown parameters, RCPE was found to be robust to the choice of hyperparameters and parameter initialization. Finally, for the case where three density measurements were used to estimate three unknown parameters, of the six possible choices of permutation matrices, only one was found to be successful.

Downloaded by UNIV OF MICHIGAN on July 23, 2022 | http://arc.aiaa.org | DOI: 10.2514/1.1010819

Acknowledgments

This research was supported by the U.S. Air Force Office of Scientific Research under Dynamic Data-Driven Applications Systems grant FA9550-16-1-0071. We thank the reviewers for helpful comments that improved this paper.

References

[1] Ljung, L., "Asymptotic Behavior of the Extended Kalman Filter as a Parameter Estimator for Linear Systems," *IEEE Transactions on Automatic Control*, Vol. 24, No. 1, 1979, pp. 36–50. https://doi.org/10.1109/TAC.1979.1101943

[2] Plett, G. L., "Extended Kalman Filtering for Battery Management Systems of LiPB-Based HEV Battery Packs—Part 3. State and Parameter Estimation," *Journal of Power Sources*, Vol. 134, No. 2, 2004, pp. 277–292. https://doi.org/10.1016/j.jpowsour.2004.02.033

[3] Van der Merwe, R., and Wan, E. A., "The Square-Root Unscented Kalman Filter for State and Parameter-Estimation," *Proceedings of IEEE International Conference on Acoustics, Speech, and Signal Processing*, Vol. 6, IEEE, New York, 2001, pp. 3461–3464. https://doi.org/10.1109/ICASSP.2001.940586

[4] Wan, E. A., and Van Der Merwe, R., "The Unscented Kalman Filter for Nonlinear Estimation," *Adaptive Systems for Signal Processing, Communications, and Control Symposium*, IEEE, New York, 2000, pp. 153–158. https://doi.org/10.1109/ASSPCC.2000.882463

[5] Evensen, G., "The Ensemble Kalman Filter for Combined State and Parameter Estimation," *IEEE Control Systems Magazine*, Vol. 29, No. 3, 2009, pp. 83–104. https://doi.org/10.1109/MCS.2009.932223

[6] Madankan, R., Singla, P., Singh, T., and Scott, P. D., "Polynomial-Chaos-Based Bayesian Approach for State and Parameter Estimations," *Journal of Guidance, Control, and Dynamics*, Vol. 36, No. 4, 2013, pp. 1058–1074. https://doi.org/10.2514/1.58377

[7] Simon, D., *Optimal State Estimation: Kalman, H-Infinity, and Nonlinear Approaches*, Wiley, Hoboken, NJ, 2006.

[8] Evensen, G., *Data Assimilation: The Ensemble Kalman Filter*, Springer, New York, 2009.

[9] Jaakkola, T. S., and Jordan, M. I., "Bayesian Parameter Estimation via Variational Methods," *Statistics and Computing*, Vol. 10, No. 1, 2000, pp. 25–37. https://doi.org/10.1023/A:1008932416310

[10] Raffard, R. L., Amonlirdviman, K., Axelrod, J. D., and Tomlin, C. J., "An Adjoint-Based Parameter Identification Algorithm Applied to Planar Cell Polarity Signaling," *IEEE Transactions on Automatic Control*, Vol. 53, Jan. 2008, pp. 109–121. https://doi.org/10.1109/TAC.2007.911362

[11] Eknes, M., and Evensen, G., "Parameter Estimation Solving a Weak Constraint Variational Formulation for an Ekman Model," *Journal of Geophysical Research: Oceans*, Vol. 102, No. C6, 1997, pp. 12479–12491. https://doi.org/10.1029/96 JC03454

[12] Goel, A., and Bernstein, D. S., "Gradient-, Ensemble-, and Adjoint-Free Data-Driven Parameter Estimation," *Journal of Guidance, Control, and Dynamics*, Vol. 42, No. 3, 2019, pp. 1085–1096. https://doi.org/10.2514/1.J055812

[13] Ridley, A. J., Deng, Y., and Toth, G., "The Global Ionosphere–Thermosphere Model," *Journal of Atmospheric and Solar-Terrestrial Physics*, Vol. 68, No. 8, 2006, pp. 839–864. https://doi.org/10.1016/j.jastp.2006.01.008

[14] Bougher, S., Pawlowski, D., Bell, J., Nelli, S., McDunn, T., Murphy, J., Chizek, M., and Ridley, A., "Mars Global Ionosphere-Thermosphere Model: Solar Cycle, Seasonal, and Diurnal Variations of the Mars Upper Atmosphere," *Journal of Geophysical Research: Planets*, Vol. 120, No. 2, 2015, pp. 311–342. https://doi.org/10.1002/2014 JE004715

[15] Roble, R., Ridley, E. C., Richmond, A., and Dickinson, R., "A Coupled Thermosphere/Ionosphere General Circulation Model," *Geophysical Research Letters*, Vol. 15, No. 12, 1988, pp. 1325–1328. https://doi.org/10.1029/GL015i012p01325

[16] Pavlov, A., "Diffusion and Thermodiffusion of Atmospheric Neutral Gases: A Review," *Surveys in Geophysics*, Vol. 40, No. 2, 2019, pp. 247–276. https://doi.org/10.1007/s10712-019-09522-2

[17] Morozov, A. V., Ridley, A. J., Bernstein, D. S., Collins, N., Hoar, T. J., and Anderson, J. L., "Data Assimilation and Driver Estimation for the

Global Ionosphere–Thermosphere Model Using the Ensemble Adjustment Kalman Filter," *Journal of Atmospheric and Solar-Terrestrial Physics*, Vol. 104, Nov. 2013, pp. 126–136. https://doi.org/10.1016/j.jastp.2013.08.016

[18] Pawlowski, D. J., and Ridley, A. J., "The Effect of the Characteristics of Solar Flares on the Thermospheric Response," *AGU Fall Meeting Abstracts*, 2009, https://ui.adsabs.harvard.edu/abs/2009AGUFMSA51A1213P/abstract.

[19] Schunk, R. W., and Nagy, A. F., *Ionospheres*, Cambridge Univ. Press, New York, 2004.

[20] Pavlov, A. V., "Thermal Conductivity of the Multicomponent Neutral Atmosphere," *Journal of Geophysical Research: Space Physics*, Vol. 122, No. 12, 2017, pp. 12–476. https://doi.org/10.1002/2017 JA024397

[21] Bellman, R., and Åström, K. J., "On Structural Identifiability," *Mathematical Biosciences*, Vol. 7, Nos. 3–4, 1970, pp. 329–339. https://doi.org/10.1016/0025-5564(70)90132-X

[22] Grewal, M., and Glover, K., "Identifiability of Linear and Nonlinear Dynamical Systems," *IEEE Transactions on Automatic Control*, Vol. 21, No. 6, 1976, pp. 833–837. https://doi.org/10.1109/TAC.1976.1101375

[23] Stanhope, S., Rubin, J. E., and Swigon, D., "Identifiability of Linear and Linear-in-Parameters Dynamical Systems from a Single Trajectory," *SIAM Journal on Applied Dynamical Systems*, Vol. 13, No. 4, 2014, pp. 1792–1815. https://doi.org/10.1137/130937913

[24] Mareels, I. M. Y., Bitmead, R. R., Gevers, M., Johnson, C. R., Kosut, R. L., and Poubelle, M. A., "How Exciting Can a Signal Really Be?" *Systems and Control Letters*, Vol. 8, No. 3, 1987, pp. 197–204. https://doi.org/10.1016/0167-6911(87)90027-2

[25] Willems, J. C., Rapisarda, P., Markovsky, I., and De Moor, B. L., "A Note on Persistency of Excitation," *Systems and Control Letters*, Vol. 54, No. 4, 2005, pp. 325–329. https://doi.org/10.1016/j.sysconle.2004.09.003

J. P. How
Associate Editor

Downloaded by UNIV OF MICHIGAN on July 23, 2022 | http://arc.aiaa.org | DOI: 10.2514/1.1010819